crystals

MDPI

Article

Theoretical Study on (*n*,*n*)-Nanotubes Rolled-up from B/N Substituted Me-Graphene

Hong-Chao Luo [1,2], Feng-Yin Li [1], Ya-Nan Zhang [1,*], Hong-Xing Zhang [1,*], Roberts I. Eglitis [3] and Ran Jia [1,3,*]

[1] College of Chemistry, Jilin University, Changchun 130023, China
[2] School of Science, Shenyang Aerospace University, Shenyang 110136, China
[3] Institute of Solid State Physics, University of Latvia, LV1067 Riga, Latvia
* Correspondence: zhangyn@jlu.edu.cn (Y.-N.Z.); zhanghx@jlu.edu.cn (H.-X.Z.); jiaran@jlu.edu.cn (R.J.); Tel.: +86-431-8849-8966 (R.J.)

Abstract: In this work, the (n,n)-type nanotube systems rolled up from the B/N substituted Me-graphene (i.e., Me-CBNT and Me-CNN, respectively) were investigated with the aid of the density functional theory (DFT). Due to the lattice dynamic instabilities until $n = 10$, the $(n,0)$ and (n,m) nanotube systems were not involved in this study. According to our calculations at the Perdew-Burke-Ernzerhof (PBE) level, the (n,n) Me-CBNT and Me-CNNT systems possess excellent mechanical strengths. The Young's moduli of Me-CBNTs can reach 60% of single-walled carbon nanotubes (SWCNTs), while their mass densities are only around 70% of SWCNTs. Based on the fully relaxed geometric configurations at the PBE level, the electronic configurations of the related nanotubes were evaluated by using the global hybrid functional B3LYP with 36% Fock exchanges. The (n,n) Me-CBNTs are metallic, while the (n,n) Me-CNNTs are semiconductors with the inherent band gaps in the range of 3.08 eV to 3.31 eV. The Bloch flat bands appear on both sides of their Fermi levels, indicating the localized charge carriers. Their band edge arrangements imply that these materials are promising candidates for the photocatalytic water splitting reactions at certain pH values.

Keywords: Me-graphene; nanotube; substitution; bloch flat band; DFT

Citation: Luo, H.-C.; Li, F.-Y.; Zhang, Y.-N.; Zhang, H.-X.; Eglitis, R.I.; Jia, R. Theoretical Study on (*n*,*n*)-Nanotubes Rolled-up from B/N Substituted Me-Graphene. *Crystals* **2023**, *13*, 829. https://doi.org/10.3390/cryst13050829

Academic Editor: Thomas M. Klapötke

Received: 16 April 2023
Revised: 15 May 2023
Accepted: 15 May 2023
Published: 17 May 2023

1. Introduction

The four valence electrons in the outer shell of a carbon atom may hybridize into sp, sp^2, and sp^3 states to form a variety of allotropes. In the recent two decades, the low-dimensional carbon materials have attracted great attention in the research community owing to their excellent mechanical strength and unique electronic features. Many two-dimensional (2D) carbon allotropes beyond graphene have already been successfully synthesized, e.g., carbon ene-yne graphyne [1,2], γ-graphyne [3–5], graphdiyne [6,7], and Biphenylene network [8]. There are even more theoretical proposals for the 2D carbon allotropes with sterling physical natures, e.g., α- and β-graphynes [9], 6,6,12-graphyne [10], pentagraphene [11], pentahexoctite [12], T-graphene [13], octagraphene [14], and so on.

Generally, the 2D materials, especially the one-atomic thick ones, can easily be rolled up to form the corresponding nanotube systems with further reduced dimensions. The most famous example is, of course, the single-walled carbon nanotubes (SWCNTs) rolled up from graphene. The bending strains and chirality can modulate the band structures of certain SWCNT systems but with almost unaffected mechanical strengths [15–18]. Following this train of thought, many 2D carbon allotropes have also been rolled up to construct their 1D nanotube systems. The theoretical study on the 6,6,12-GNTs based on the monolayer 6,6,12-graphyne revealed an even–odd relation in the $(n,0)$ tubes [18]. The nanotubes rolled-up from the α-, β-, and γ-graphynes exhibit unique mechanical and electronic properties [19–23], although only γ-graphyne has been successfully synthesized thus far [3]. After the experimental synthesis of the monolayer graphdiyne [6,7], its nanotube system (GDYNT) has also been synthesized with a wall thickness of 40 nm [24]. The

GDYNT arrays possess excellent field emission performance, which is even higher than that of other semiconducting carbon nanotubes [24]. A recent study has reported that the MXene/GDYNT composite films can be used as a free-standing and flexible solid-state supercapacitor [25]. The single-walled boron nitride nanotubes (SWBNNTs) can be regarded as the counterpart of the corresponding SWCNTs, which have also been intensively studied [26–28]. Other than them, the multi-atomic thick 2D films composed of metal oxides or metal (transition-metal) sulfides have also been used to construct the nanotube systems [29–32]. TiO_2 nanotube is a typical example with significant photocatalytic performance and application potentials in the solar energy conversion field [33–35]. It is worth noting that there are usually more obvious bending effects in the tube systems based on the corresponding multi-atomic thick 2D films than that based on the one-atomic thick 2D systems with the similar tube radius because the thicker the wall of the tube system, the greater the difference between the inner and outer walls.

Very recently, a new 2D carbon allotrope, Me-graphene (or labeled as C_{568}), has also been predicted by using DFT calculations [36,37]. This material consists of both sp^3 and sp^2 carbons with $P\bar{4}m2$ symmetry. According to the GW calculation, where G represents the one-body Green's function, and W denotes the dynamically screened Coulomb interaction. Me-graphene is a semiconductor with an indirect band gap of 2.04 eV. Further investigations indicate that its physical features can be effectively regulated by stacking, strains, hydrogenation, adsorption, and many other methods [37–41]. Using Me-graphene as a template, some of new 2D materials can be designed. Substitutions of the sp^3 hybridized C-atoms in Me-graphene with certain metal atoms can significantly enhance its feasibility of working as an electrode in Li-ion batteries [42]. Especially in the Al-substituted Me-graphene, its specific energy capacity reaches 1097 mAh/g, which is almost three times that of graphite (372 mAh/g). Furthermore, the migration energy barrier on the Al-substituted Me-graphene system is very low to be considered as promising candidate for ultrafast charging system. On the other hand, the substitutions of the sp^2 C-atoms in the 5-membered rings with B-, N-, or Si-atoms lead to new 2D boron carbide (Me-C_8B_4C), carbon nitride (Me-C_8N_4C), or silicon carbide (Me-C_8Si_4C), respectively [43]. The almost flat 2D Me-C_8B_4C is actually metallic, indicating its application potential as electromagnetic shielding. Moreover, owing to the high concentration of the B-atoms in this flat system, it may also be employed as the neutron absorption material with an excellent mechanical strength. The 2D Me-C_8N_4C is a semiconductor with an inherent indirect band gap of 1.869 eV, as predicted at the HSE06 level [43], which implies its application potentials in the field of photocatalysis and energy conversion. The band structure of 2D Me-C_8N_4C is also very sensitive to the external stress. Its indirect band gap can be turned into a direct one under a moderate strain. The gap can also be linearly adjusted under strains in its elastic range to meet a wider application range. Me-graphene and its derivatives can be considered as multi-functional nanomaterials, and, thus, provide more options for high performance nanodevices.

In the present work, the so-called Me-CBNT and Me-CNNT nanotube systems are proposed by rolling-up the 2D carbides Me-C_8B_4C and Me-C_8N_4C. Considering the structural stability and our computational capability, the (n, n)-type nanotubes are carefully investigated with the aid of the DFT calculations. Their geometric configurations, mechanical strengths, and electronic configurations are systematically discussed. We hope that this study can expand the family of the nanotube materials, and provide some new ideas for their applications.

2. Materials and Methods

The majority of the calculations in this study were carried out within the framework of density functional theory (DFT) with the general gradient approximation (GGA) using the CRYSTAL17 package [44]. The full geometry relaxations (not only for the atomic configurations, but also for the lattices) of the related 1D Me-CBNT and Me-CNNT systems were performed at the Perdew-Burke-Ernzerhof (PBE) level [45], and their mechanical

features were also estimated at the same level. Note that the PBE functional was also employed in the original works for the prediction of the monolayer Me-graphene [36,37]. In order to compare the geometric configurations of the tube systems with the original 2D Me-graphene and its derivatives, the PBE functional is still used in this work for geometry optimizations. To describe one-electron states in the nanotubes, the Gaussian all-electron basis sets of triple-ζ Valence with Polarization [46] for the species related in this work were employed. A dense enough $16 \times 16 \times 1$ Monkhorst-Pack (MP) grid was set for the integral sampling in the corresponding Brillouin zones.

Considering the fact that the pure DFT functionals will always underestimate the band gap of a semiconductor, the electronic properties were evaluated with the aid of the global hybrid functional B3LYP [47] based on the optimized configurations at the PBE level. However, according to the previous studies [48,49], the original hybrid functionals, e.g., B3LYP, PBE0, and HSE06, also underestimate the band gaps of 2D materials to a certain extent. The GW method is recommended for such calculations, especially when the non-local dielectric screening effect is significant [50,51]. On the other hand, the GW method is very expensive. Therefore, considering the balance between the accuracy and computational consumption, a hybrid functional with adjusted hybridized exchange term may be a more appropriate choice. After careful testing [52], the global hybrid B3LYP functional with a 36% Fock exchange can provide an indirect band gap of 2.05 eV for the monolayer Me-graphene, which, indeed, agrees excellently with the GW result of 2.04 eV [36]. Note that the relative weights of the nonlocal parts in the exchange and correlation potentials in the employed B3LYP functional are set to be 0.90 and 0.81, respectively. Therefore, the electronic properties of the related nanotube systems in the present work were estimated with the aid of the B3LYP functional with a 36% hybrid exchange term.

3. Results

3.1. Geometric Configurations and Stabilities

The related nanotubes are actually based on the B/N substituted monolayer Me-graphene systems, where their sp^2-hybridized carbon atoms bonding with the sp^3-hybridized center carbon are replaced by the B- or N-atoms, respectively. The stabilities of these substituted Me-graphene systems (i.e., Me-C_8B_4C and Me-C_8N_4C) have been carefully verified in the previous work [43]. The lattices of the new 2D systems are still primitive tetragonal with the $P\bar{4}M2$ symmetries. The square lattice indicates that any roll-up vector for these new 2D systems is possible [53]. In other words, any (n, m) nanotubes based on the 2D Me-C_8B_4C or Me-C_8N_4C systems can be mathematically established with the corresponding periodicity along its tube axial direction. According to our previous study on the nanotubes rolled from the pristine Me-graphene [52], the physical properties of a chiral tube system (n, m) with $n \geq m$ lie just between the corresponding $(n, 0)$ and (n, n) systems. Therefore, the present work focuses only on the tube systems $(n, 0)$ and (n, n). As sketched in Figure 1, the B- and N-doped Me-graphene systems possess clearly different thicknesses, which are only 0.004 Å and 1.460 Å, respectively. The different configurations of the valence electrons on the B- and N-atoms lead to different bonding between the heteroatoms and carbons, and thus result in the different thicknesses. The energy band maps indicate that the 2D Me-C_8B_4C system is metallic, while the 2D Me-C_8N_4C system is a semiconductor. More detailed discussion about their electronic properties will be provided in the following section. In this work, the related nanotubes rolled from Me-C_8B_4C and Me-C_8N_4C are labeled as Me-CBNT and Me-CNNT, respectively. As examples, the (7, 0) and (7, 7) Me-CBNT and Me-CNNT systems are also sketched in Figure 1. In comparison with the diameters of the related nanotube systems, the (n, n) tube is naturally thicker than the $(n, 0)$ one with the same n. Considering the collapse probability of the nanotube with a large diameter [18,54], the system with a tube size $n > 30$ is not involved in the present investigation. Note that in the following discussions, the carbon atoms in the related tube systems are still labeled as sp^2- and sp^3-hybridized carbons inherited from the original monolayer Me-graphene system to identify its position in the corresponding monolayer system, although the band

bending caused by the curvature will change the degree of the orbital hybridization to some extent.

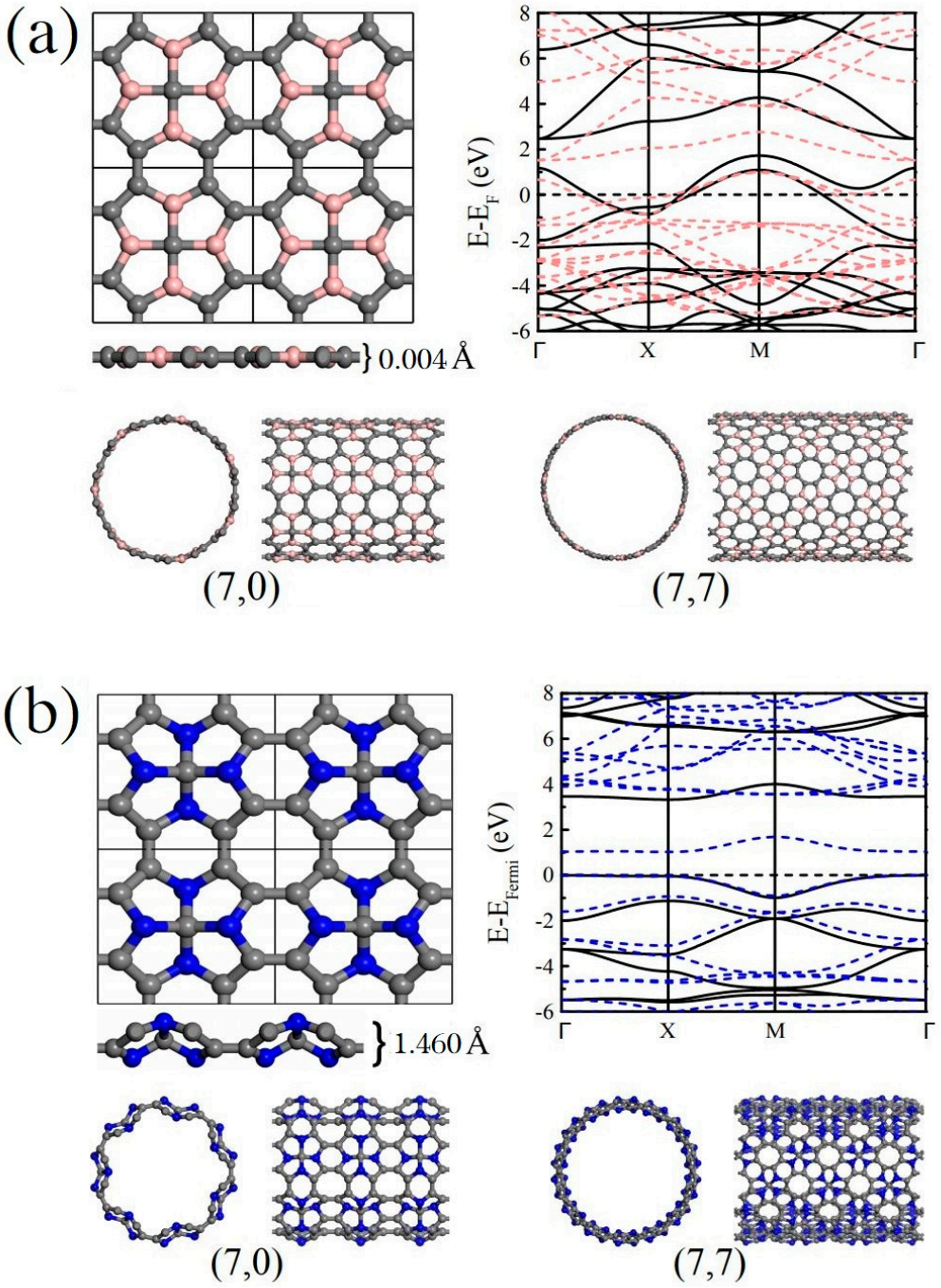

Figure 1. (**a**) Sketches for the monolayer Me-C_8B_4C and the corresponding (7, 0), (7, 7) Me-CBNTs after full geometric optimizations at the PBE level, as well as the band structure of the monolayer Me-C_8B_4C. (**b**) Sketches for the monolayer Me-C_8N_4C and the corresponding (7, 0), (7, 7) Me-CNNTs after full geometric optimizations at the PBE level, as well as the band structure of the monolayer Me-C_8N_4C. Note that in the band maps, the dashed lines are obtained from the PBE calculations, while the solid lines represent the results at the B3LYP level with 36% Fock exchange.

The cohesive energies of the related nanotubes are estimated by using the common definition as follows:

$$E_{\text{coh}} = \frac{1}{n+m}(E_{tot} - n\mu_{\text{C}} - m\mu_{\text{X}}) \quad (1)$$

where E_{tot} and μ represent the total energy of the corresponding nanotube system and the chemical potential of the C-, B-, or N-atom, respectively. The numbers of the C- and B/N-atoms are labeled as n and m, respectively. Based on our understanding, the chemical potential of a species can be influenced by many factors, such as temperature, pressure, and system composition [55]. Following the common theoretical strategy [56–58], the total energy of the isolated atom is used here to replace the corresponding chemical potential. The estimated cohesive energies of the related nanotubes are plotted in Figure 2a. The cohesive energies of the tube systems are of course higher than that of the corresponding 2D systems, while they decrease exponentially with the increases of their radii and finally approach the values of the monolayer systems. The more obvious changes of the cohesive energies of the Me-CNNT systems are caused by the bonds and bond angles between the sp^3-C and the surrounding N-atoms. The patterns of the cohesive energy curves are determined by the corresponding bending strain energies, as plotted in Figure 2b, which are estimated according to the following definition:

$$E_s = \frac{1}{m}(E_{tot} - mE_{uc}) \quad (2)$$

where E_{tot} and E_{uc} denotes the total energy of a nanotube and the energy of a unit cell of the corresponding monolayer system and m denotes the number of the used unit cells of the corresponding monolayer system, respectively. Obviously, although the radii of the $(n, 0)$ and an (m, m) Me-CNNT systems are very close (e.g., the $(10,\ 0)$ and $(7,\ 7)$ ones with the radii of 8.62 Å and 8.65 Å, respectively), the bending strain energies of the $(n, 0)$ systems are higher than that of (m, m). The extra strain energy of an $(n, 0)$ Me-CNNT occurs due to the further bending of the C–N bonds along the rolling vector. The bending strain may significantly change their electronic properties, but it also raises the possibility of structural instability. The nonmonotonic section at the small radii in Figure 2 appears in Me-CBNTs. As shown in Figure S1, the change of the wall-thickness of a Me-CBNT system is more significant. Due to the electron-deficient B-atom, the electronic structures of the Me-CBNT systems at small radii are obviously different compared with the ones with large radii, which will be clearly discussed in the following section. The change of the electronic structure of an Me-CBNT system with a small radius leads to the nonmonotonic variations of the cohesive and strain energies. Moreover, the strain energy of the Me-CBNT system with a large radius fluctuates obviously as shown in the inset in Figure 2b. However, it should be noted that these values are almost zero at large radii. Thus, this fluctuation is, in fact, a calculation error.

The phonon dispersion relations of the related Me-CBNT and Me-CNNT systems confirm the instability raised by the excessive strain energies. As exhibited in Figure S2, the lattice dynamic stabilities of both $(n, 0)$ Me-CBNT and Me-CNNT systems cannot yet be satisfied even with a large tube size $n = 10$. Generally, the vibration branch with negative frequencies is also called as soft mode in solid state physics. Along the soft mode, the lattice of the related system can find another configuration with even lower energy. Therefore, a phonon map with soft mode can be used to confirm the instability of the corresponding system from the lattice dynamic perspective. Considering the affordability of our computational consumption, the further discussion on the $(n, 0)$-type systems is therefore abandoned in this work. As exhibited in Figure 3, the thinnest (n, n) Me-CBNT and Me-CNNT with lattice stabilities are the $(4,\ 4)$ and $(6,\ 6)$ ones with the radii of 5.499 Å and 7.420 Å, respectively. It can be certain that the other Me-CBNT and Me-CNNT systems with respective larger tube sizes should also be lattice dynamic stable due to their even smaller bending strain energies. The instability of a related tube system with small radius is mainly caused by the large curvature. As shown in Figure 2b, the strain energy increases significantly with a small tube radius. On the other hand, the strain energy of an (n, 0) tube system (not only Me-CNNTs but also Me-CBNTs) is obviously higher than that of the corresponding (m, m) one with the similar radius. Of course, there are also some other

influences caused by the electron redistribution, which is actually still the result led by the bending strain.

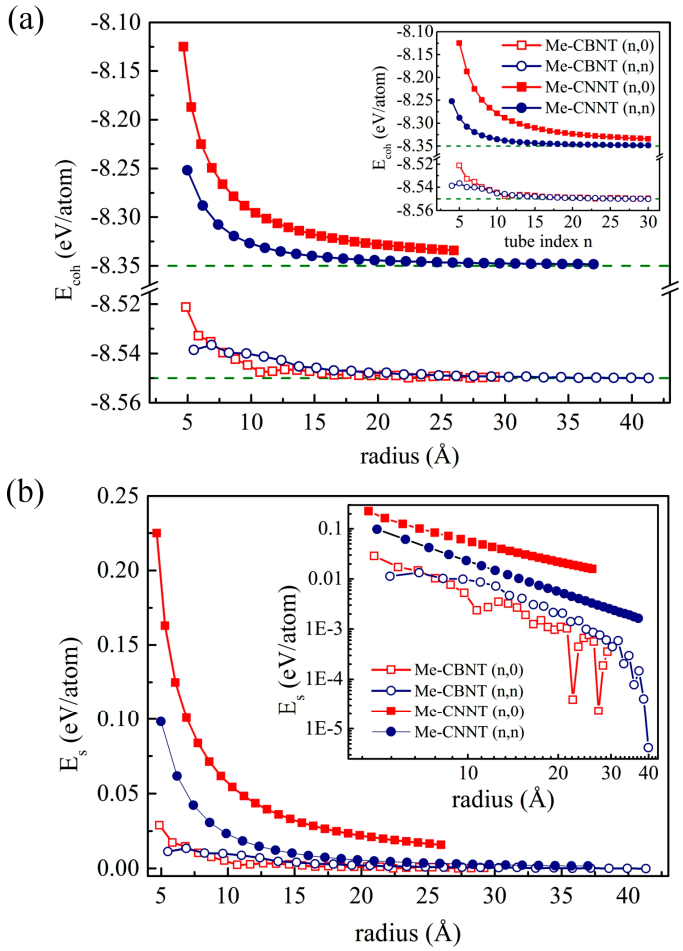

Figure 2. (**a**) The cohesive energy profiles and (**b**) the strain energy profiles of the related Me-CBNT and Me-CNNT as functions of the tube radius at the PBE level. Note that the corresponding profiles as functions of the tube index *n* are also exhibited as insets.

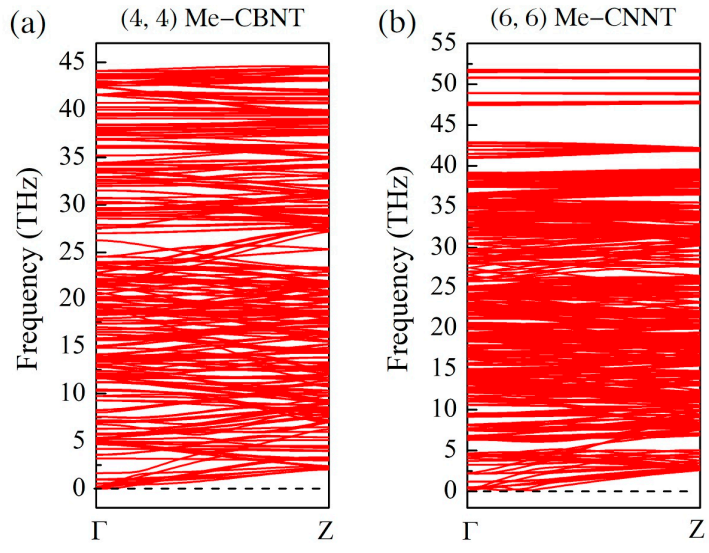

Figure 3. The phonon dispersion relation maps for (**a**) the (4, 4) Me-CBNT and (**b**) the (6, 6) Me-CNNT, obtained at the PBE level.

3.2. Mechanical Properties

For a 1D nanotube system, its mechanical strength can be evaluated by using its Young's modulus:

$$Y_{1D} = \frac{1}{2\pi rhl}\frac{\partial^2 E}{\partial \varepsilon^2} = \frac{C_{1D}}{2\pi rh} \quad (3)$$

where E represents the total energy, ε denotes the uniaxial strain, and C_{1D} is the elastic constant for the 1D system. r, h, and l represent the radius, wall-thickness, and length of the unit cell of a nanotube, respectively. The effective cross-section of a nanotube system is actually not readily obtainable. The key point is the definition of its wall thickness. In this work, the wall thickness h is defined as the sum of the geometric wall thickness d of the corresponding nanotube and the distance 3.40 Å of the conventional van der Waals interaction, i.e., $h = d + 3.40$ Å. The geometric wall thicknesses d of the related nanotube systems are plotted as functions of the tube index n in Figure S1.

The positive Young's modulus, or, rather, the positive elastic constant, already satisfies the Born-Huang criteria for a 1D system, which implies its mechanical stability. Similar to SWCNTs [18], the mechanical strengths of the Me-CBNT and Me-CNNT systems are not significantly related to the curvature as shown in Figure 4, when the tube sizes are not particularly small, especially the Me-CNNT systems. The Young's modulus of an (n, n) Me-CNNT is almost a constant, regardless of the increasing tube index n, because its geometric wall thickness reaches the value of the 2D Me-C_8N_4C system (around 1.460 Å) after $n = 9$ and remains almost unchanged in the following data, as exhibited in Figure S1. The corresponding stable value is around 462 GPa, which is even about 4.5% higher than the Young's modulus of the 2D Me-C_8N_4C system (around 442 GPa). On the contrary, the geometric wall thickness of an Me-CBNT system with a relatively large curvature becomes obviously larger than that of the monolayer Me-C_8B_4C, as plotted in Figure S1. However, this single factor (in comparison with the relatively large van der Waals distance 3.40 Å) cannot bring a significant mechanical degradation, as shown in Figure 4. Although the Young's modulus of an Me-CBNT finally approaches 600 GPa, it is only about 70% of the monolayer Me-C_8B_4C (around 868 GPa). This significant degradation is actually caused by the reduction of the attenuations of the C–B bonds due to the electron redistributions during rolling up. The electron redistributions of the related systems will be discussed in the following section. It is worth mentioning that the mass densities of Me-CBNTs and Me-CNNTs are around 1.55 g/cm^3 and 1.87 g/cm^3, respectively, which are lower than the density of the monolayer graphene (around 2.25 $\sim$ 2.27 g/cm^3) [59,60]. Therefore, the reported nanotube systems, especially Me-CBNTs, can be considered as strong and lightweight 1D materials.

3.3. Electronic Properties

Trivially, the strain, caused not only by axial stress but also by bending, can lead to electron redistributions to some extent. The effective charges of the atoms in the related nanotubes are qualitatively evaluated by using Hirshfield-I analysis, while the overlap populations on the covalent bonds are estimated with Mulliken analysis. In the smallest Me-CBNT case, i.e., (4, 4) Me-CBNT, the large curvature leads to more charge transfer by around 12 me from the B atoms to the central sp^3-C atom. The B atom donates 504 me to the adjacent C-atoms in (4, 4) Me-CBNT due to its low electronegativity. Although the overlap population between the B atom and the sp^3-C atom remains almost unchanged, the corresponding bond length is reduced by around 0.009 Å. Moreover, considering the direction of the rolling vector, there are three different C–C bonds between the sp^2-C atoms, i.e., the one perpendicular and the one parallel to the axial direction, as well as the rest bonds in the 8-membered carbon ring. Note that the C–C bonds perpendicular and parallel to the tube axis belong to the 5- and 8-membered rings at the same time, while the others belong to the 6- and 8-membered rings. In (4, 4) Me-CBNT, the parallel C–C bonds are slightly shorted but with reduced overlap populations from 364 me to 344 me, implying the strength reduction of this covalent bond. Moreover, the overlap populations on all

B–C bonds also reduce several millielectrons in comparison with the values in the flat Me-C_8B_4C system. The bond angle $\angle BCB$ also reduces from 179.82° in the 2D system to 168.30°, resulting in the change of its geometric wall thickness. The general reductions of the overlap populations on the effectively stressed chemical bonds and the increase of the wall thickness imply the decline of the mechanical strength of an Me-CBNT. On the other side, in $(6, 6)$ Me-CNNT, the effective charges of the N- and C-atoms, the average bond lengths, and the overlap populations remain almost unchanged in comparison with that in the 2D Me-C_8N_4C system. Moreover, the bond angle $\angle NCN$ is increased by only around 5.59° from 122.09° in the corresponding 2D Me-C_8N_4C system. These factors avoid the significant loss of the mechanical strength of Me-CNNT. To more intuitively present the changes of the configurations caused by the curvatures of the tube systems, the changed bond lengths and angles in the $(4, 4)$ Me-CBNT and $(6, 6)$ Me-CNNT systems are sketched in Figure S3, while as references for comparisons, the bond lengths and angles in the corresponding monolayer Me-C_8B_4C and Me-C_8N_4C systems are also illustrated in Figure S3.

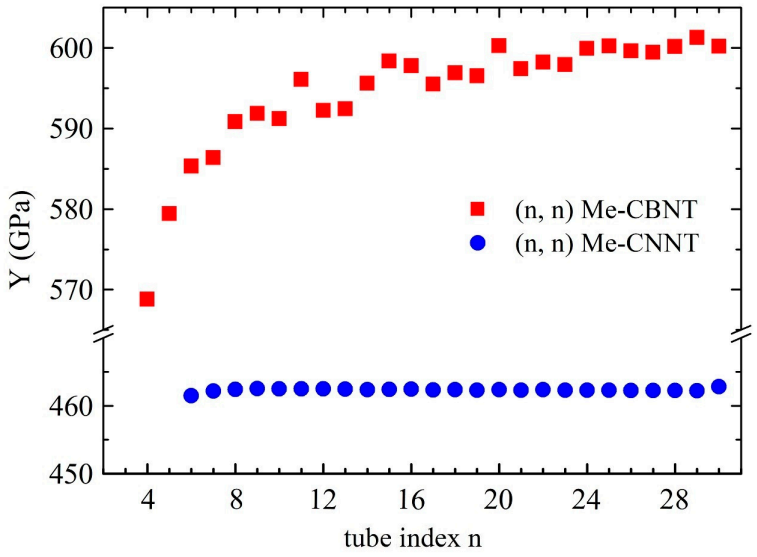

Figure 4. The Young's moduli of the (n, n) type Me-CBNTs and Me-CNNTs as functions of the tube index n estimated at the PBE level.

According to our previous study [52], the global hybrid functional B3LYP with 36% Fock exchange term can provide a reasonable band structure of Me-graphene with the band gap of 2.05 eV, which agrees excellently with the GW result of 2.04 eV [36]. The further calculations based on this strategy indicate that the 2D Me-C_8B_4C is metallic, while the 2D Me-C_8N_4C is a semiconductor with a direct band gap of 3.32 eV. For convenience, the hybridization ratio (36%) of the employed B3LYP will not be emphasized in the following at the PBE level, the bending strain does not open a band gap for Me-CBNT (as exhibited in Figure 5a), while the band gaps of Me-CNNTs are reduced to some extent (as shown in Figure 5b). The change of the band gaps of (n, n) Me-CNNTs is plotted in Figure 6a as a function of tube index n. The gap exponentially increases from 3.08 eV to 3.31 eV as its curvature decreases approaching the 2D one. These band gaps fall into the visible light range. Moreover, the variations of the band gaps are mainly caused by the changes of VBMs, as exhibited in Figure 6b. The density of states (DOSs) profiles of the $(4, 4)$ Me-CBNT and $(6, 6)$ Me-CNNT systems are the same as the examples illustrated in Figure 7a,b respectively. The $(4\,4)$ Me-CBNT system is metallic. The bands near its Fermi level are mainly from the sp^2 hybridized C-atoms. In the semiconducting $(6, 6)$ Me-CNNT system, the conduction band minimum (CBM) is mainly from the sp^2 hybridized C-atoms, while the valence band maximum (VBM) is contributed by the sp^2 C-atoms and the N-atoms together. Furthermore, the band edges of the 1D (n, n) Me-CNNTs are extremely flat,

as exhibited in the band maps in Figure 6b. This is actually inherited from the 2D Me-C_8N_4C, as reported in our previous work [43]. The similar Bloch flat bands have also been predicted in a polar twisted bilayer h-BN system with a twist angle smaller than 3.89° [61]. In advantage, the Bloch flat bands are inherent in 1D (n, n) Me-CNNTs without moiré superlattices. The flat band edges in Me-CNNTs indicate the diverging effective masses of their charge carriers with vanished group velocities in the high temperature phase. Therefore, a large binding energy of the excitons in such systems can be expected and result in the self-trapped excitons. Apparently, this will lead to difficulties in carrier separation. The non-dispersive flat bands are mainly caused by the absence of localized dielectric screening in low-dimensional systems. However, considering the practical applications, the surrounding water molecules, solvents, and the adjacent materials in a nanotube bundle or composite system can provide enough screening effects to effectively abate the binding energy of excitons.

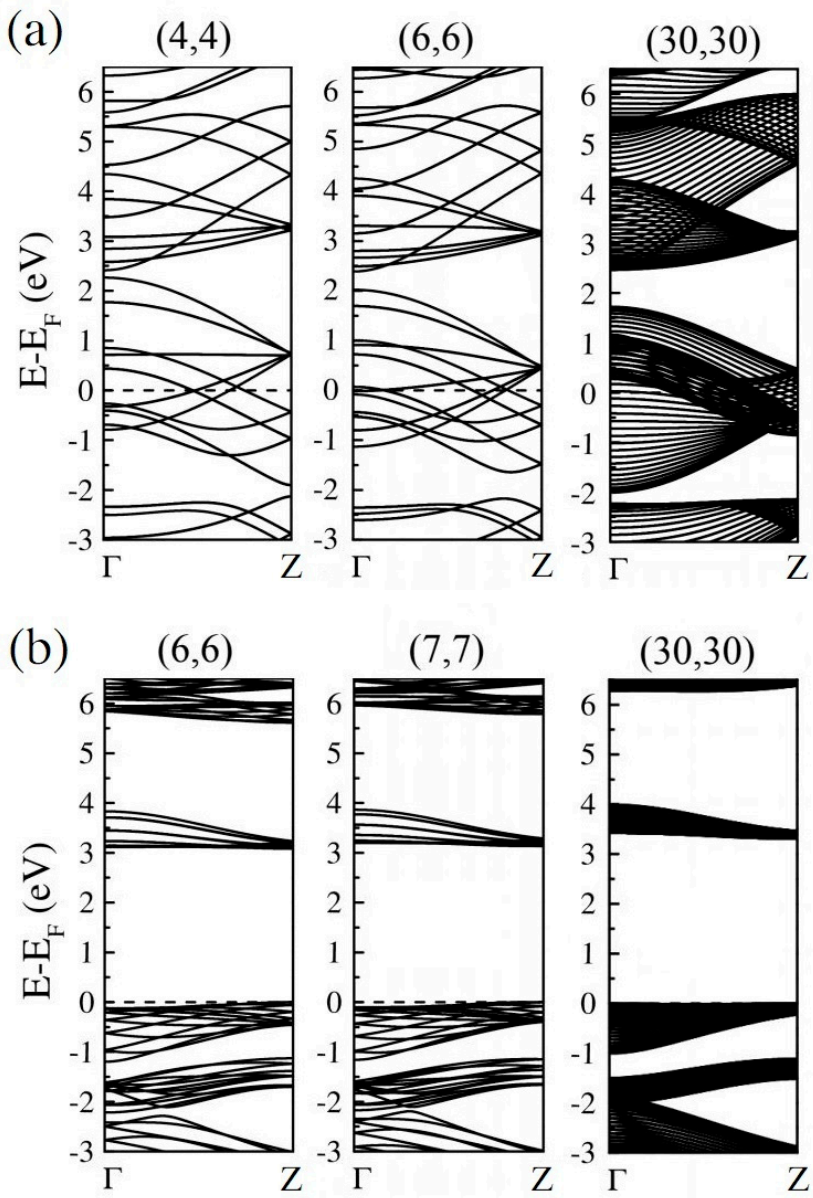

Figure 5. The band structures of some typical (**a**) metallic (n, n) Me-CBNTs and (**b**) semiconducting (n, n) Me-CNNTs as examples obtained at the B3LYP level. Note that the Fermi levels are all shifted to zero.

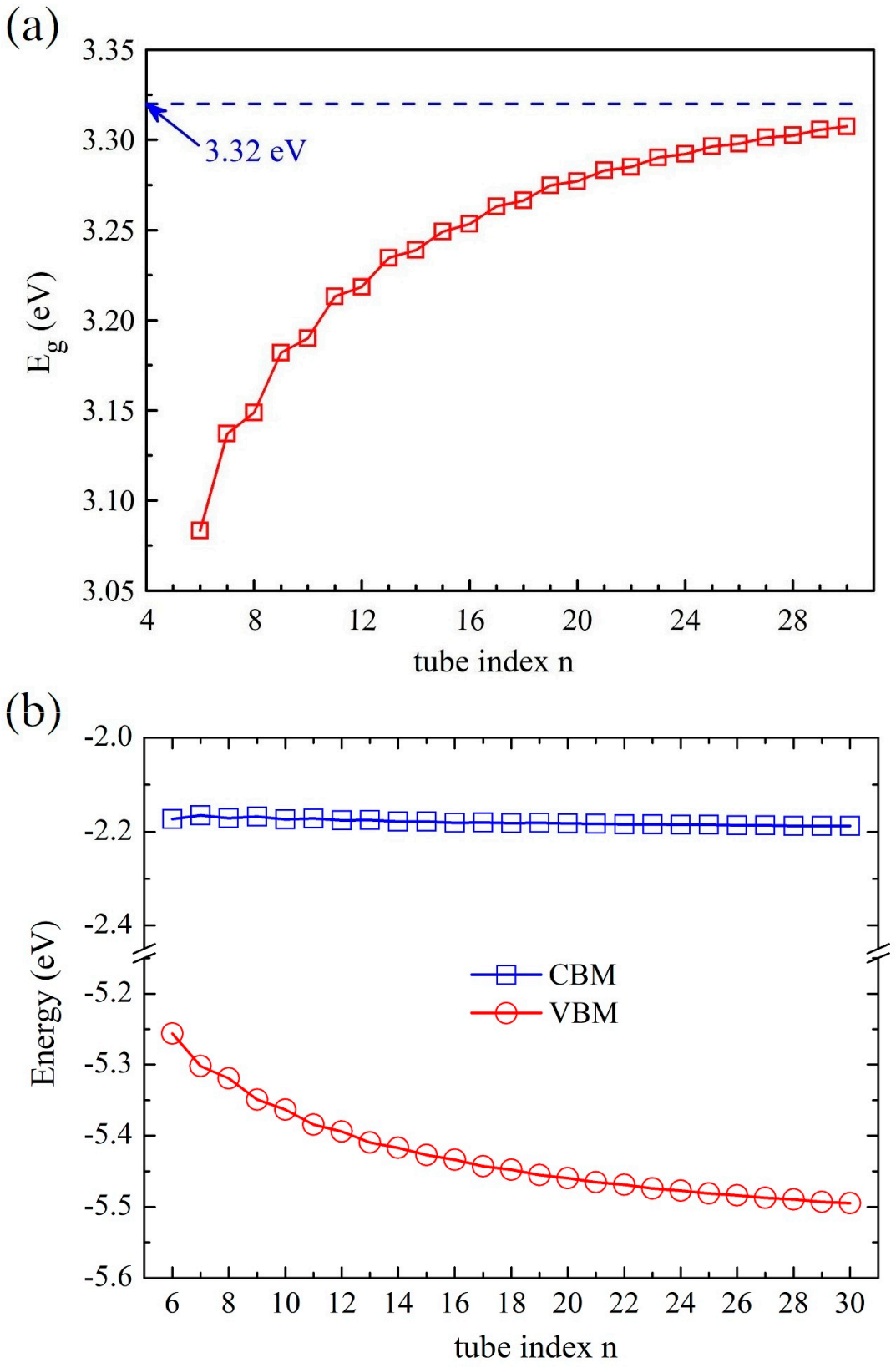

Figure 6. (**a**) The variations of the band gaps of the (n, n) Me-CNNT and (**b**) the band edge arrangements of the (n, n) Me-CNNT as functions of the tube index n. All data are obtained at the B3LYP level.

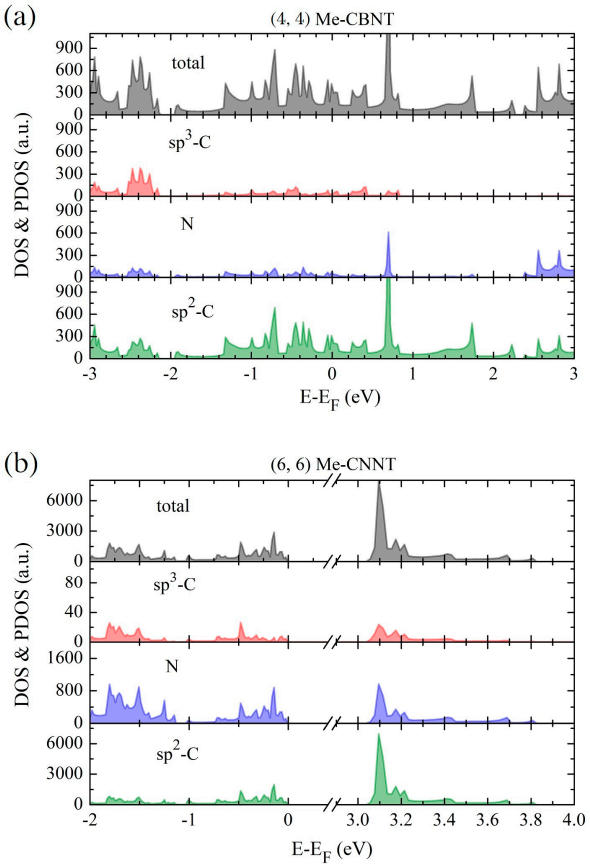

Figure 7. The profiles of the total density of states (DOSs) and the projected density of states (PDOSs) for (**a**) the (4, 4) Me-CBNT and (**b**) (6, 6) Me-CNNT estimated at the B3LYP level. Note that the Fermi levels are also shifted to zero.

4. Conclusions

In summary, the (n, n) type nanotubes rolled up from the 2D Me-C_8B_4C and Me-C_8N_4C systems (i.e., Me-CBNT and Me-CNNT) were studied with the aid of the DFT calculations. Their geometric and electronic configurations were systematically discussed until the tube index $n = 30$. Considering the structural instabilities with $n \leq 10$ and the huge computational consummations, the $(n, 0)$ type nanotubes were discarded in the present work. According to the analyses of the phonon dispersion relations, the thinnest Me-CBNT and Me-CNNT are the (4, 4) and (6, 6) ones with the radii of 5.499 Å and 7.420 Å, respectively. The related nanotubes exhibit high mechanical strengths with low mass densities. The Young's moduli of Me-CBNTs, especially, can even reach 60% of SWCNTs, but with only 70% the mass density of SWCNTs. Based on the fully relaxed geometric configurations of the related nanotubes at the pure PBE level, their electronic configurations were evaluated by using the global hybrid functional B3LYP but with 36% hybridization. Following this strategy, the calculation results indicate that the (n, n) Me-CBNTs are all metallic, while the (n, n) Me-CNNTs are semiconductors with flat band edges. According to their band gaps varied in 3.08∼3.31 eV, the (n, n) Me-CNNTs can be considered as promising candidates for the solar energy applications. We hope that this work can bring some new ideas for the further developments of low-dimensional materials.

Supplementary Materials: The following supporting information can be downloaded at: https://www.mdpi.com/article/10.3390/cryst13050829/s1, Figure S1: The thicknesses of the tube walls as functions of the tube index n; Figure S2: The phonon dispersion relations of the related Me-CBNT and Me-CNNT (n, 0) systems. The profiles are obtained after full relaxations at the PBE level; Figure S3: The comparison of the bond lengths and angles between the tube systems and the corresponding 2D systems.

Author Contributions: Investigation, Visualization, Writing original draft, H.-C.L. Investigation, Visualization, F.-Y.L. Validation, Writing-review editing, Y.-N.Z. Supervision, Resources, H.-X.Z. Supervision, Data curation, R.I.E. Conceptualization, Supervision, Writing-review editing, R.J. All authors have read and agreed to the published version of the manuscript.

Funding: The Institute of Solid State Physics, University of Latvia (Latvia) as the Centre of Excellence has received funding from the European Union's Horizon 2020 Frame-work Programme H2020-WIDESPREAD-01-2016-2017-Teaming Phase 2 under grant agreement No. 739508, project CAMART-2.

Institutional Review Board Statement: Not applicable.

Informed Consent Statement: Not applicable.

Data Availability Statement: The data presented in this study are available on request from the corresponding author.

Conflicts of Interest: The authors declare no conflict of interest.

References

1. Mortazavi, B.; Shahrokhi, M.; Rabczuk, T.; Pereira, L.F.C. Electronic, optical and thermal properties of highly stretchable 2D carbon Ene-yne graphyne. *Carbon* **2017**, *123*, 344–353. [CrossRef]
2. Jia, Z.; Zuo, Z.; Yi, Y.; Liu, H.; Li, D.; Li, Y.; Li, Y. Low temperature, atmospheric pressure for synthesis of a new carbon Ene-yne and application in Li storage. *Nano Energy* **2017**, *33*, 343–349. [CrossRef]
3. Li, Q.; Li, Y.; Chen, Y.; Wu, L.; Yang, C.; Cui, X. Synthesis of γ-graphyne by mechanochemistry and its electronic structure. *Carbon* **2018**, *136*, 248–254. [CrossRef]
4. Li, Q.; Yang, C.; Wu, L.; Wang, H.; Cui, X. Converting benzene into γ-graphyne and its enhanced electrochemical oxygen evolution performance. *J. Mater. Chem. A* **2019**, *7*, 5981–5990. [CrossRef]
5. Hu, Y.; Wu, C.; Pan, Q.; Jin, Y.; Lyu, R.; Martinez, V.; Huang, S.; Wu, J.; Wayment, L.J.; Clark, N.A.; et al. Synthesis of γ-graphyne using dynamic covalent chemistry. *Nat. Synth.* **2022**, *1*, 449–454. [CrossRef]
6. Li, Y.; Xu, L.; Liu, H.; Li, Y. Graphdiyne and graphyne: From theoretical predictions to practical construction. *Chem. Soc. Rev.* **2014**, *43*, 2572–2586. [CrossRef]
7. Gao, X.; Liu, H.; Wang, D.; Zhang, J. Graphdiyne: Synthesis, properties, and applications. *Chem. Soc. Rev.* **2019**, *48*, 908–936. [CrossRef]
8. Fan, Q.; Yan, L.; Tripp, M.W.; Krejčí, O.; Dimosthenous, S.; Kachel, S.R.; Chen, M.; Foster, A.S.; Koert, U.; Liljeroth, P.; et al. Biphenylene network: A nonbenzenoid carbon allotrope. *Science* **2021**, *372*, 852–856. [CrossRef]
9. Puigdollers, A.R.; Alonso, G.; Gamallo, P. First-principles study of structural, elastic and electronic properties of α-, β- and γ-graphyne. *Carbon* **2016**, *96*, 879–887. [CrossRef]
10. Malko, D.; Neiss, C.; Vines, F.; Görling, A. Competition for Graphene: Graphynes with Direction-Dependent Dirac Cones. *Phys. Rev. Lett.* **2012**, *108*, 086804. [CrossRef]
11. Zhang, S.; Zhou, J.; Wang, Q.; Chen, X.; Kawazoe, Y.; Jena, P. Penta-graphene: A new carbon allotrope. *Proc. Natl. Acad. Sci. USA* **2015**, *112*, 2372–2377. [CrossRef] [PubMed]
12. Sharma, B.R.; Manjanath, A.; Singh, A.K. Pentahexoctite: A new two-dimensional allotrope of carbon. *Sci. Rep.* **2014**, *4*, 7164. [CrossRef] [PubMed]
13. Liu, Y.; Wang, G.; Huang, Q.; Guo, L.; Chen, X. Structural and Electronic Properties of *T* Graphene: A two-Dimensional carbon allotrope with tetrarings. *Phys. Rev. Lett.* **2012**, *108*, 225505. [CrossRef] [PubMed]
14. Sheng, X.L.; Cui, H.J.; Ye, F.; Yan, Q.B.; Zheng, Q.R.; Su, G. Octagraphene as a versatile carbon atomic sheet for novel nanotubes, unconventional fullerenes, and hydrogen storage. *J. Appl. Phys.* **2012**, *112*, 074315. [CrossRef]
15. Lu, J.P. Elastic Properties of Carbon Nanotubes and Nanorope. *Phys. Rev. Lett.* **1997**, *79*, 1297–1300. [CrossRef]
16. Salvetat-Delmotte, J.P.; Rubio, A. Mechanical properties of carbon nanotubes: A fiber digest for beginners. *Carbon* **2002**, *40*, 1729–1734. [CrossRef]
17. Lee, C.; Wei, X.; Kysar, J.W.; Hone, J. Measurement of the Elastic Properties and Intrinsic Strength of Monolayer Graphene. *Science* **2008**, *321*, 385–388. [CrossRef]
18. Yang, D.C.; Jia, R.; Wang, Y.; Kong, C.P.; Wang, J.; Ma, Y.; Eglitis, R.I.; Zhang, H.X. Novel Carbon Nanotubes Rolled from 6,6,12-Graphyne: Double Dirac Points in 1D Material. *J. Phys. Chem. C* **2017**, *121*, 14835–14844. [CrossRef]

19. Faria, B.; Silvestre, N.; Lopes, J.N. Strength and fracture of graphyne and graphdiyne nanotubes. *Comp. Mater. Sci.* **2020**, *171*, 109233. [CrossRef]
20. Coluci, V.R.; Braga, S.F.; Legoas, S.B.; Galvão, D.S.; Baughman, R.H. Families of carbon nanotubes: Graphyne-based nanotubes. *Phys. Rev. B* **2003**, *68*, 035430. [CrossRef]
21. Coluci, V.R.; Braga, S.F.; Legoas, S.B.; Galvão, D.S.; Baughman, R.H. New families of carbon nanotubes based on graphyne motifs. *Nanotechnology* **2004**, *15*, 142–149. [CrossRef]
22. Zhao, H.; Wei, D.; Zhou, L.; Shi, H.; Zhou, X. Thermal conductivities of graphyne nanotubes from atomistic simulations. *Comp. Mater. Sci.* **2015**, *106*, 69–75. [CrossRef]
23. Kang, B.; Lee, J.Y. Electronic properties of α-graphyne nanotubes. *Carbon* **2015**, *84*, 246–253. [CrossRef]
24. Li, G.; Li, Y.; Qian, X.; Liu, H.; Lin, H.; Chen, N.; Li, Y. Construction of tubular molecule aggregations of graphdiyne for highly efficient field emission. *J. Phys. Chem. C* **2011**, *115*, 2611–2615. [CrossRef]
25. Wang, Y.; Chen, N.; Liu, Y.; Zhou, X.; Pu, B.; Qing, Y.; Zhang, M.; Jiang, X.; Huang, J.; Tang, Q.; et al. MXene/Graphdiyne nanotube composite films for Free-Standing and flexible Solid-State supercapacitor. *Chem. Eng. J.* **2022**, *450*, 138398. [CrossRef]
26. Chopra, N.G.; Luyken, R.J.; Cherrey, K.; Crespi, V.H.; Cohen, M.L.; Louie, S.G.; Zettl, A. Boron Nitride Nanotubes. *Science* **1995**, *269*, 966–967. [CrossRef]
27. Golberg, D.; Bando, Y.; Tang, C.C.; Zhi, C.Y. Boron Nitride Nanotubes. *Adv. Mater.* **2007**, *19*, 2413–2432. [CrossRef]
28. Wang, J.; Lee, C.H.; Yap, Y.K. Recent advancements in boron nitride nanotubes. *Nanoscale* **2010**, *2*, 2028–2034. [CrossRef]
29. Allam, N.K.; Shankar, K.; Grimes, C.A. A General Method for the Anodic Formation of Crystalline Metal Oxide Nanotube Arrays without the Use of Thermal Annealing. *Adv. Mater.* **2008**, *20*, 3942–3946. [CrossRef]
30. Chen, X.; Unruh, K.M.; Ni, C.; Ali, B.; Sun, Z.; Lu, Q.; Deitzel, J.; Xiao, J.Q. Fabrication, Formation Mechanism, and Magnetic Properties of Metal Oxide Nanotubes via Electrospinning and Thermal Treatment. *J. Phys. Chem. C* **2011**, *115*, 373–378. [CrossRef]
31. Li, H.; Chen, S.; Zhang, Y.; Zhang, Q.; Jia, X.; Zhang, Q.; Gu, L.; Sun, X.; Song, L.; Wang, X. Fabrication, Systematic design of superaerophobic nanotube-array electrode comprised of transition-metal sulfides for overall water splitting. *Nat. Commun.* **2018**, *9*, 2452. [CrossRef] [PubMed]
32. Yu, X.Y.; Yu, L.; Lou, X.W. Metal Sulfide Hollow Nanostructures for Electrochemical Energy Storage. *Adv. Energy Mater.* **2016**, *6*, 1501333. [CrossRef]
33. Hahn, R.; Schmidt-Stein, F.; Salonen, J.; Thiemann, S.; Song, Y.; Kunze, J.; Lehto, V.-P.; Schmuki, P. Semimetallic TiO_2 Nanotubes. *Angew. Chem. Int. Ed.* **2009**, *48*, 7236–7239. [CrossRef]
34. Roy, P.; Berger, S.; Schmuki, P. TiO_2 Nanotubes: Synthesis and Applications. *Angew. Chem. Int. Ed.* **2011**, *50*, 2904–2939. [CrossRef]
35. Ge, M.; Li, Q.; Cao, C.; Huang, J.; Li, S.; Zhang, S.; Chen, Z.; Zhang, K.; Al-Deyab, S.S.; Lai, Y. One-dimensional TiO_2 Nanotube Photocatalysts for Solar Water Splitting. *Adv. Sci.* **2017**, *4*, 16001.
36. Zhuo, Z.; Wu, X.; Yang, J. Me-graphene: A graphene allotrope with near zero Poisson's ratio, sizeable band gap, and high carrier mobility. *Nanoscale* **2020**, *12*, 19359–19366. [CrossRef]
37. Ram, B.; Mizuseki, H. C_{568}: A new two-dimensional sp^2-sp^3 hybridized allotrope of carbon. *Carbon* **2020**, *158*, 827–835. [CrossRef]
38. Gao, Q.; Sahin, H.; Kang, J. Strain tunable band structure of a new 2D carbon allotrope C_{568}. *J. Semicond.* **2020**, *41*, 082005. [CrossRef]
39. Marinho, E.; da Silva Autreto, P.A. Me-graphane: Tailoring the structural and electronic properties of Me-graphene via hydrogenation. *Phys. Chem. Chem. Phys.* **2021**, *23*, 9483–9491. [CrossRef]
40. Yang, Y.; Zhang, G.; Zhu, Y.; Peng, X.; He, L. Electronic properties of hydrogen/fluorine adsorbed two-dimensional C_{568}: A first-principles study. *Surf. Interfaces* **2022**, *31*, 102067. [CrossRef]
41. Sampaio-Silva, A.; Ferreira, D.F.; Silva, C.A.B., Jr.; Del Nero, J. Hydrogenation, width and strain effect in Me-graphene devices. *Comp. Mater. Sci.* **2022**, *210*, 111456. [CrossRef]
42. Zhao, W.H.; Li, F.Y.; Zhang, H.X.; Eglitis, R.I.; Wang, J.; Jia, R. Dopingat at sp^3-site in Me-graphene(C_{568}) for new anodes in rechargeable Li-ion battery. *Appl. Surf. Sci.* **2023**, *607*, 154895. [CrossRef]
43. Zhao, W.H.; Zhang, J.Q.; Zhang, H.X.; Wang, J.; Jia, R. 2D Boron Carbide, Carbon Nitride, and Silicon Carbide: A Theoretical Prediction. ACS Appl. *Electron. Mater.* **2022**, *4*, 4903–4911. [CrossRef]
44. Dovesi, R.; Erba, A.; Orlando, R.; Zicovich-Wilson, C.M.; Civalleri, B.; Maschio, L.; Rérat, M.; Casassa, S.; Baima, J.; Salustro, S.; et al. Quantum-Mechanical Condensed Matter Simulations with CRYSTAL. *WIREs Comput. Mol. Sci.* **2018**, *8*, e1360. [CrossRef]
45. Perdew, J.P.; Burke, K.; Ernzerhof, M. Generalized Gradient Approximation Made Simple. *Phys. Rev. Lett.* **1996**, *77*, 3865–3868. [CrossRef] [PubMed]
46. Laun, J.; Vilela Oliveira, D.; Bredow, T. Consistent gaussian basis sets of double- and triple-zeta valence with polarization quality of the fifth period for solid-state calculations. *J. Comput. Chem.* **2018**, *39*, 1285–1290. [CrossRef]
47. Becke, A.D. Density-functional thermochemistry. III The role of exact exchange. *J. Chem. Phys.* **1993**, *98*, 5648. [CrossRef]
48. Li, M.; Reimers, J.R.; Ford, M.J.; Kobayashi, R.; Amos, R.D. Accurate prediction of the properties of materials using the CAM-B3LYP density functional. *J. Comput. Chem.* **2021**, *42*, 1486–1497. [CrossRef]
49. Allec, S.I.; Wong, B.M. Inconsistencies in the Electronic Properties of Phosphorene Nanotubes: New Insights from Large-Scale DFT Calculations. *J. Phys. Chem. Lett.* **2016**, *7*, 4340–4345. [CrossRef]
50. Yi, Z.J.; Wu, M.; Pang, Y.; Jia, R.; Xu, R.R. Non-local dielectric screening effects in phosphorene/g-C_3N_4 heterojunctions. *Appl. Surf. Sci.* **2021**, *567*, 150842. [CrossRef]

51. Yi, Z.; Wu, M.; Jia, R. Edge modified phosphorene nanoribbon heterojunctions: Promising metal-free photocatalysts for direct overall water splitting. *J. Mater. Sci.* **2022**, *57*, 5482–5496. [CrossRef]
52. Luo, H.C.; Li, F.Y.; Zhao, W.H.; Zhang, H.X.; Eglitis, R.I.; Chen, J.; Jia, R. Carbon nanotubes rolled from Me-graphene. *Diam. Relat. Mater.* **2023**, *135*, 109845. [CrossRef]
53. Li, F.Y.; Eglitis, R.I.; Zhang, H.X.; Jia, R. Reasonable BN nanotubes composed of B–B and N–N bonds: A theoretical prediction. *Appl. Surf. Sci.* **2023**, *608*, 155156. [CrossRef]
54. Gao, G.; Cagin, T.; Goddard III, W.A. Energetics, structure, mechanical and vibrational properties of single-walled carbon nanotubes. *Nanotechnology* **1998**, *9*, 184–191. [CrossRef]
55. Reuter, K.; Scheffler, M. Composition, structure, and stability of RuO_2 (110) as a function of oxygen pressure. *Phys. Rev. B* **2001**, *65*, 035406. [CrossRef]
56. Wang, K.; Shi, C.; Zhao, N.; Du, X.; Li, J. First-principles study of the B- or N-doping effects on chemical bonding characteristics between magnesium and single-walled carbon nanotubes. *Chem. Phys. Lett.* **2009**, *469*, 145–148. [CrossRef]
57. Zhou, J.Q.; Li, L.; Fu, C.; Wang, J.; Fu, P.; Kong, C.P.; Bai, F.Q.; Eglitis, R.I.; Zhang, H.X.; Jia, R. A novel T-C_3N and seawater desalination. *Nanoscale* **2020**, *12*, 5055–5066. [CrossRef]
58. Fu, P.; Yang, D.C.; Jia, R.; Yi, Z.J.; Liu, Z.F.; Li, X.; Eglitis, R.I.; Su, Z.M. Metallic subnanometer porous silicon: A theoretical prediction. *Phys. Rev. B* **2021**, *103*, 014117. [CrossRef]
59. Zhang, Z.W.; Liu, Z.Y.; Xiao, B.L.; Ni, D.R.; Ma, Z.Y. High efficiency dispersal and strengthening of graphene reinforced aluminum alloy composites fabricated by powder metallurgy combined with friction stir processing. *Carbon* **2018**, *135*, 215–223. [CrossRef]
60. Li, X.; Palazzolo, A. A review of flywheel energy storage systems: State of the art and opportunities. *J. Energy Storage* **2022**, *46*, 103576. [CrossRef]
61. Zhao, X.J.; Yang, Y.; Zhang, D.B.; Wei, S.H. Formation of Bloch Flat Bands in Polar Twisted Bilayers without Magic Angles. *Phys. Rev. Lett.* **2020**, *124*, 086401. [CrossRef] [PubMed]